Revision 1

Partition behavior of platinum-group elements during the segregation of arsenide melts from sulfide magma

Rubén Piña[1,*], Fernando Gervilla[2], Hassan Helmy[3], Raúl O.C. Fonseca[4], and Chris Ballhaus[5]

[1] Departamento de Mineralogía y Petrología, Facultad de Ciencias Geológicas, Universidad Complutense de Madrid, c/ José Antonio Novais s/n, 28040 Madrid, Spain

* Corresponding author, email: rpinagar@ucm.es; 0034-91-3944882

[2] Departamento de Mineralogía y Petrología and Instituto Andaluz de Ciencias de la Tierra, Facultad de Ciencias, Universidad de Granada-CSIC, Avda. Fuentenueva s/n, 18002 Granada, Spain

[3] Department of Geology, Minia Universitu, 61519 Minia, Egypt

[4] Institut für Geologie und Mineralogie, Universität zu Köln, 50674 Köln, Germany

[5] Steinmann Institut, Universität Bonn, 53115-Bonn, Germany

Abstract Evidence of immiscibility between arsenide and sulfide melts has been observed both in experimental studies and natural samples from several localities worldwide (e.g., Ronda, Spain; Beni Bousera, Morocco; Dundonald Beach South, Canada). Platinum-group elements (PGE) have shown to have a strong affinity for arsenide melts but little is known about their partitioning behavior between arsenide and sulfide melts. In this study, we experimentally determine the partition coefficients of PGE (Pt, Pd, Ir, Ru and Os) between both types of melt in As-saturated sulfide systems doped with trace amounts of PGE. Results show that all PGE display a strong preference to the arsenide melt with $D_{PGE}^{(arsenide\ melt/sulfide\ melt)}$ ranging from 20 to 2700, with Ir and Pt showing a marked preference for arsenide melts. These partition coefficients values are similar to estimates made from natural samples and demonstrate that the separation of arsenide melts from sulfide magmas can be an efficient mechanism to scavenge PGE from magmas and to fractionate Os, Ru and Pd from Pt and Ir.

Key-words: PGE, arsenide melt, sulfide melt, liquid immiscibility, LA-ICP-MS, partition coefficients.

Introduction

Since 90's, several experimental studies have demonstrated the existence of liquid immiscibility between arsenide and sulfide melts at magmatic temperatures (850-1200 ºC) (Makovicky et al. 1990, 1992; Fleet et al. 1993; Tomkins 2010; Helmy et al. 2010, 2013a; Sinyakova and Kosyakov 2012). These studies have further showed that arsenide melts are efficient collectors of platinum-group elements (PGE, Os, Ir, Ru, Rh, Pt and Pd) because these metals are strongly concentrated into arsenides once arsenide melt is segregated from the original sulfide liquid. This mechanism of liquid immiscibility has successfully explained the formation of PGE-enriched arsenide and sulfarsenide minerals in close spatial relation with Fe-Ni-Cu sulfide minerals in a number of magmatic sulfide ores (Gervilla et al. 1996, 1998; Hanley 2007; Power et al. 2004; Godel et al. 2012; Piña et al. 2013, 2015; Moroni et al. 2017). Certainly, arsenide melt immiscibility is an uncommon process observed only in a few locations due to the unusually high As concentrations required in the sulfide magmas to segregate an arsenide melt. Indeed, As is a trace element in mafic-ultramafic magmas and typical basaltic magmas remain well below As saturation even after extensive crystallization (e.g., Wood 2003). However, As is relatively enriched in the crust, particularly in sedimentary rocks, for which the incorporation of external As into the ore-forming melts is considered to be fundamental for arsenide immiscibility.

Although experimental and empirical works cited above clearly highlight that arsenide melts have profound effects on the distribution of PGE, little is known about the partition behavior of PGE between both arsenide and sulfide melts, particularly in the case of IPGE (i.e., Os, Ir, and Ru). Wood (2003) estimated a minimum partition coefficient for Pd between arsenide and sulfide melt ($D_{Pd}^{As/sulf}$) of 34. Hanley (2007) and Godel et al. (2012) inferred $D_{PGE}^{As/sulf}$ of the order of 10-100 in the high-grade Pd and Pt sulfide mineralization of Dundonald Beach South (Ontario) and 25-400 in the Rosie Prospect (Western Australia), respectively. Piña et al. (2013) estimated $D_{PGE}^{As/sulf}$ ranging from 50 to 920, using PGE abundances in co-existing arsenide and sulfide minerals (formed from arsenide and sulfide melts, respectively) from the Amasined Ni-Cu ores (Beni Bousera, North Morocco). All these values undoubtedly reflect the extent to which the presence of arsenide melts influence PGE behavior during sulfide crystallization, but it is necessary to better constrain their real magnitude and possible differences between the PGE group.

The objective of the present study is to quantitatively determine the partition coefficients of PGE between discrete arsenide and sulfide melts. These values have been obtained by carrying out an experimental study where arsenide and sulfide melts have been equilibrated over a temperature range of 1200 to 1000 ºC from an arsenide-saturated Co-Ni-Cu-Fe sulfide mix doped with trace amounts of PGE. In addition, we have tested how PGE behave during the slow cooling of the arsenide melt until temperature of 840 ºC. Although we know that natural sulfide melts do not have the high amounts of As used in these experiments, these were driven to generate large amounts of arsenide melts and observe unequivocally PGE partitioning behavior. Our results show that behavior of PGE is quite consistent with observations in natural samples with significantly lower amounts of arsenides.

Arsenide-sulfide immiscibility in natural occurrences

Liquid immiscibility between arsenide and sulfide melts has been documented in several magmatic sulfide ores (e.g., Ronda, Spain, Gervilla et al. 1996, Piña et al. 2015; Amasined mineralization, Beni Bousera massif, Morocco, Gervilla et al. 1996, Piña et al. 2013; Kylmäkoski deposit, Finland, Gervilla et al. 1998; Dundonald Beach South deposit, Canada, Hanley 2007; Talnotry deposit, Scotland, Power et al. 2004; Rosie Nickel prospect, Australia, Godel et al. 2012; Wannaway komatiite-hosted Ni sulfide deposit, Kambalda, Australia, Moroni et al. 2017). Among all these occurrences, the chromite-Ni arsenide mineralization of the Serranía de Ronda (Spain) probably represents the most interesting example due to its unique metallogeny and the wellpreserved textural evidence of arsenide-sulfide immiscibility. We refer the reader to a book review by Gervilla et al (2019) for complete view of the mineralization. The peridotite massifs of the Serranía de Ronda host two types of unique magmatic mineralization in the world (Oen et al. 1979; Leblanc et al. 1990; Gervilla and Leblanc 1990): 1) Cr-Ni mineralization composed of chromite and Ni arsenides (mainly, nickeline NiAs, maucherite $Ni_{11}As_8$, and nickeliferous löllingite $FeAs_2$) singularly enriched in PGE and Au, and 2) mineralization consisting of Fe-Ni-Cu sulfides and graphite with minor chromite, hereafter sulfide-graphite (S-G) mineralization. Whole-rock PGE concentrations are significantly higher in the Cr-Ni mineralization (1,260 ± 530 ppb) than in the S-G ores (340 ± 190 ppb) (Leblanc et al. 1990). In general, the richest the mineralization is in Ni arsenide, the highest total contents of PGE are. In addition, the high bulk rock abundances of PGE do not have mineralogical expression as platinum-group minerals. By contrast, LA-ICP-MS analyses in individual arsenide grains of the Cr-Ni ores showed that all arsenides contain high concentrations of PGE, particularly in Ir, Rh and Pt, whereas coexisting sulfide minerals are strongly depleted in these noble metals (Piña et al. 2015). It is suggested that Cr-Ni and S-G ores were genetically linked as the two immiscible arsenide and sulfide melt that were segregated from a common As- and S-rich melt (Gervilla and Leblanc 1990; Gervilla et al. 1996). Textural evidence supporting arsenide-sulfide immiscibility include the existence of sulfides forming separate layers of pyrrhotite-chromite intercalated in the massive chromite-nickeline (± löllingite) ore (Fig. 1a), the coexistence of arsenide and sulfide domains with typical magmatic textures against chromite and silicate minerals (Fig 1b), and composite exsolution lamellae of pyrrhotite, pentlandite and chalcopyrite in nickeline and vice versa.

In a similar geodynamic context to the Serranía de Ronda, the Amasined Cr-Ni mineralization from Beni Bousera lherzolite massif, Morocco, consists of 20-30 meters long and up to one-meter thick lens of massive sulfides formed by pyrrhotite, pentlandite and chalcopyrite, and chromite. Arsenide minerals are concentrated in a 5-10 cm thick, basal zone along the footwall of the massive sulfides. They consist mostly of radially fractured, lobular or rounded maucherite globules within pyrrhotite (Fig. 1c-d, Piña et al. 2013). Locally, maucherite globules include early-crystallized chromite crystals that could have been trapped into arsenide melt. Maucherite contains significant amounts of all PGE (77-195 ppm), whereas coexisting sulfides are invariably poor in these metals (< 1 ppm). The presence of maucherite inclusions in mss can be explained if immiscible arsenides melt was present prior to mss crystallization from a sulfide liquid. In addition, maucherite is enriched in elements compatible with MSS, such as Re, Os, Ir, Ru and Rh, which also indicates that arsenide immiscibility took place before MSS crystallization.

Methods

Experimental set-up

The starting composition (in wt. %) for each experiment consists of 43.8 Fe, 10.8 Ni, 3.8 Cu, 0.9 Co, 13.8 As and 26.9 S. This mixture is doped by 60 ppm of each of the PGE (Os, Ru, Ir, Pt and Pd). The starting concentrations of As and PGE were high and low enough, respectively, to guarantee the separation of large enough amounts of arsenide melt suitable for laser ablation analyses, and to avoid the early saturation of discrete PGM such as sperrylite. The mixture was prepared by first adding PGE, as hydrochloric and/or nitric acid solutions, to the elemental sulfur fraction. After drying at 60 °C overnight to evaporate the carrier solutions, Fe, Ni, Cu, Co and As are added to the sulfur as metal powders. The mix is ground thoroughly in an agate mortar, placed inside 6-mm outer diameter SiO_2 glass tubes, welded shut at 1 Pa, then pre-reacted by slow heating to 700 °C to form a homogeneous sulfide phase. After regrinding the prereacted sulfide, five charges, each filled with a 175 mg aliquots of the starting composition, are welded in evacuated SiO_2 glass tubes and then reacted at the designated run temperature until equilibrium is reached. The duration of the 1200, 1100 and 1000 °C experimental runs was set to 6, 12, 24 hours, respectively, which have been shown to be long enough for equilibrium to be reached (Helmy et al. 2010; Helmy and Bragagni 2017; Helmy and Fonseca 2017). Each experiment was subsequently quenched by dropping it into a beaker filled with cold water. The 840 °C run was heated to 1100 °C for two hours and slowly cooled over 12 hours to the designed temperature and stayed there for 48 hours.

Equilibrium conditions between coexisting phases were confirmed based on the compositional homogenization of phases. Specifically, grains in the same sample have a narrow compositional range in major elements and line analyses by laser ablation ICP-MS across single grains showed the absence of heterogeneity in major and trace elements.

Sulfur fugacity (fS_2) was not strictly controlled in the experiments but its value was estimated using the composition of MSS in the run products. We have used the experimental calibration of Toulmin and Barton (1964), which relates the atomic proportion between Fe and S in MSS and fS_2 for a given temperature value, with the modifications introduced by Mengason et al. (2010) to account for the presence of Ni, Cu and Co in MSS. The estimated log fS_2 for 1000 ºC and 840 ºC was -3.5 and -6.3, respectively, that corresponds to around 1.6 and 3 log units lower relative to the Pt-PtS buffer.

Analytical methods

Run products were examined and analyzed on polished epoxy mounts for major elements (Fe, Ni, Co, Cu, As, and S) with a JEOL JXA 8200 electron microprobe at the University of Bonn (Germany) at 15kV and 15 nA, using native Ni, Co, canyon Diablo troilite, chalcopyrite, and arsenopyrite as standard reference materials for peak to background calibration. During the analyses of MSS, arsenide melt and sulfide melt, the electron beam was defocused to 30 µm to integrate small-scale chemical heterogeneities caused by quench exsolution. Matrix corrections were carried out employing the ZAF correction algorithm, to account for the different electron absorption properties between experimental phases and the reference material used.

Samples were also studied by Field Emission Scanning Electron Microprobe using a JEOL JSM 7600F at the University Complutense of Madrid (Spain) with the aim of identifying the presence of possible nanometer-size bearing PGE-As particles with arsenide and sulfide run products. This technique allows identifying nanometer-sized discrete particles on the surface of samples, which were not observed.

Trace element abundances in run products were measured using a Resonetics M50-E ATL excimer 193 nm laser coupled to a Thermo Scientific X-Series 2 quadrupole ICP-MS (Steinmann Institute, University of Bonn, Germany), following a similar procedure described by Helmy and Fonseca (2017). Count rates of ^{33}S, ^{34}S, ^{56}Fe, ^{59}Co, ^{60}Ni, ^{63}Cu, ^{65}Cu, ^{75}As, ^{100}Ru, ^{101}Ru, ^{105}Pd, ^{106}Pd, ^{108}Pd, ^{188}Os, ^{189}Os, ^{190}Os, ^{191}Ir, ^{192}Os, ^{193}Ir, and ^{195}Pt, were measured. Count rates were then normalized to the internal standard ^{57}Fe. Normalized count-rates were subsequently converted to concentrations using an in-house synthetic pyrrhotite reference material (for PGE - Bragagni et al. 2018) and NIST-SRM 610 glass (for As – Jochum et al. 2011) as the external reference standards. Any eventual baseline drift was corrected by carrying out measurements via standard-sample bracketing, whereby a block of standards was measured after every ten unknowns. Laser spot sizes were set to between 44 and 75 μm to integrate as much as possible the coarse quench textures that characterize the sulfide melt, as well as to maximize measurement sensitivity. The laser repetition rate was set to 5 Hz, and the laser fluence was measured at ca. 4.5 J/cm^2. No significant molecular or isobaric interferences were identified. Where more than one isotope of an element is analyzed (e.g. Fe, Ni, Cu, Ru, Pd) abundance ratios closely matched the natural isotope abundances. Palladium and Ru concentrations in either phase were generally high enough that any ^{65}Cu^{40}Ar interference on ^{105}Pd, of ^{60}Ni^{40}Ar and ^{61}Ni^{40}Ar on ^{100}Ru and ^{101}Ru, respectively, were negligible. This is also supported by the good agreement between the Pd and Ru concentrations obtained from the count rates of all Pd and Ru isotopes measured.

Results

Phase relations

Immiscible arsenide melt globules have been noted in experiments over the whole temperature range. The size of the globules differs according to the run temperature. No discrete PGE phases (e.g., PGM) were noted in any run experiment.

At 1200 and 1100 ºC (exp1200 and exp1100, respectively), arsenide melt occurs as randomly distributed micrometer-sized droplets within a matrix of sulfide (Fig. 2a-d). Fine-grained arsenide melt droplets predominate over several hundred micrometer-sized, rounded droplets. Detailed observations in the arsenide-sulfide melt interface seem to show the presence of “blebs” of arsenide melt migrating to the larger bleb of arsenide melt (Fig. 3). Probably, these blebs were trapped in transit due to quenching.

At 1000 ºC (exp1000), arsenide melt coexists with sulfide melt and monosulfide solid solution (MSS) (Fig. 2e-f). As in the experiments at higher temperature, arsenide melt occurs as micrometer-sized droplets, now quenched into dendritic textures. However, the arsenide melt typically occurs as a single population of 50-100 µm-sized rounded to sub-rounded globules. This texture resembles that observed by Helmy et al. (2010) in run products of experiments in the Fe-Cu-Pt-Pd-As-S system where droplets of Pd-rich arsenide melt coexist in equilibrium with MSS and sulfide melt. In detail, electron microprobe images reveal the presence of tiny arsenide melt droplets enclosed within sulfide melt (Fig. 2e-f). Interestingly, these droplets do not occur in MSS, suggesting that this phase did not entrain arsenide melt during its crystallization. It is probable that the crystallization of MSS from sulfide melt may have resulted in the coalescence of arsenide melt in relatively large single droplets. Additionally, the presence of fine-grained arsenide melt droplets within interstitial sulfide melt likely suggests that arsenide melt continued segregating from sulfide melt after MSS crystallization at temperatures close to 1000 ºC. Sulfide melt clearly locates interstitially to MSS (Fig. 2f).

In the slowly cooled 840 ºC run (exp840), two phases develop in the arsenide melt: Co-bearing arsenide phase coexisting with Ni-rich, Co-poor arsenide melt (Fig. 4a). The homogeneous appearance and composition and the sharp contact with the Co-poor melt suggest that the Co-rich phase is a stable crystalline phase. At this temperature, MSS and intermediate solid solution (ISS) are the stable sulfide phases (Fig. 4b).

Phase chemistry and base metal and PGE partition coefficients

A summary of major element concentrations (Fe, Ni, Cu, Co, As, and S) and Os, Ir, Ru, Pd and Pt in the run products is provided in Table 1 and 2, respectively (set of individual analyses is listed in Appendix 1 and 2). The major element distribution in coexisting phases in the experiments exp1100, exp1000 and exp840 is shown in different compositional X-ray maps in Figure 5.

Arsenide melt is mostly a mixture of Ni (~ 25-32 wt. %), As (~ 43-47 wt. %) with lesser amounts of Fe (~ 12-19 wt. %), S (~ 5-8 wt. %), Cu (~ 2-4 wt. %), and Co (~ 1-2 wt. %). Metal/(As+S) molar ratios range from 1.03 to 1.17. In all runs, arsenide melt is richer in Ni, As and Co, and poorer in Fe, Cu and S than coexisting sulfide melt (Fig. 6). Nickel and Co contents increase with decreasing run temperature, suggesting that these metals were progressively incorporated into the arsenide melts from sulfides on cooling (Fig. 6a-b). In contrast, S and Fe have opposite behavior decreasing their abundance in the arsenide melt with decreasing temperature (Fig. 6c-d). Between 1000 and 1200 ºC, As content in the arsenide melt remains almost constant around 45 wt. % (Fig. 6e). The contents of all PGE in the arsenide melt are much higher than in the coexisting sulfide melt (Fig. 7). The PGE content in the arsenide melt of exp1100 is slightly higher than in exp1200.

Nickel and Co are compatible in the arsenide melt with $D^{\text{arsenide melt/sulfide melt}}$ ranging from 6.6 ± 0.8 at 1200 ºC and 4.2 ± 0.5 at 1100 ºC for Ni, and around 2 for Co for both temperatures (Table 3). Copper and Fe are incompatible in the arsenide melt: $D_{Cu}^{\text{arsenide melt/sulfide melt}}$ around 0.55, and $D_{Fe}^{\text{arsenide melt/sulfide melt}} = 0.30 \pm 0.02$. The distribution of these base metals between arsenide and sulfide melts is consistent with previous studies. For example, Helmy et al. (2013a) found that the affinities of base metals for immiscible arsenide melt follow the order Ni >> Fe = Cu. In their experiments, which focused on studying phase relations in the As-bearing Fe-Ni-Cu system, Helmy et al. (2013a) noted that Ni prefers arsenide melt to sulfide melt, whereas Cu shows the opposite behavior. The high affinity of Ni with arsenide melt is also consistent with the mineral paragenesis dominated by Ni arsenide minerals (nickeline, maucherite) found in As-rich Ni-Cu sulfide deposits in Beni Bousera and Ronda (Gervilla et al. 1996; Piña et al. 2013), as well as in other magmatic sulfide ores such as Kabanga where disseminated mineralization with high As contents includes abundant nickeline (Evans et al. 1999).

All PGE are strongly compatible with the arsenide melt, with Ir and Pt showing the highest partition coefficients ($D^{As/sulf}_{Ir}$ ≈ 170-510; $D^{As/sulf}_{Pt}$ ≈ 135-2750, Table 3). Osmium and Ru have D values lower to 100, and Pd shows low positive values in exp1200 and exp1100, $D^{As/sulf}_{Pd} = 25$ and 38 respectively, but relatively high in exp1000 ($D^{As/sulf}_{Pd} = 475$). In general, the partition coefficients of PGE increase with decreasing temperature from 1200 to 1000 ºC probably reflecting the degree of separation between the arsenide and sulfide melt. As shown in Figure 2, at 1200 ºC there are many tiny arsenide droplets (probably nano-size) in the sulfide melt. At 1100 ºC, the separation is better with tiny arsenide melt droplets coalescing to micron-size droplets. Finally, in the experiment at 1000 ºC, arsenide and sulfide melt already seem to be well separated. Evidently, the smaller arsenide droplets there are inside the sulfide melt, the higher Pt and Pd is measured in the (average) sulfide melt, which lead to lower $D^{As/sulf}_{PGE}$. Nevertheless, partition coefficients of Pt and Pd show a large increase in the experiment at 1000 ºC, more than 10 times the value at 1100 ºC, not observed in Os, Ir and Ru (Table 3). It is noteworthy that the PGE showing such large increase are Pt and Pd, metals incompatible during the MSS crystallization, the solid phase present in exp1000 that does not appear at higher temperatures when MSS had not crystallized yet. At 1100 ºC, sulfide melt contains higher amounts of Pt and Pd than MSS and sulfide melt at 1000 ºC (Table 2). Unlike Os, Ir and Ru, it seems that Pt and Pd were not accommodated into MSS nor in the residual sulfide liquid, but were probably incorporated into the arsenide melt.

The As content of MSS is constant, around 0.2 wt. %, in similar fashion to what has been previously reported by Helmy et al. (2013a) for experiments carried out over a similar temperature range. The estimated $D_{As}^{MSS/sulf}$ is 0.6 ± 0.2 (Table 3). Relatively lower $D_{As}^{MSS/sulf}$ were determined by Helmy et al (2010) ($D_{As}^{MSS/sulf}$ = 0.4-0.01) and Liu and Brenan (2015) ($D_{As}^{MSS/sulf}$ = 0.1) in sulfide mixes containing traces of As. The estimated partition coefficient of Ni between MSS and sulfide melt at 1000 ºC is 0.9 ± 0.1 for an atomic metal/S ratio of MSS averaging 0.98. $D_{Ni}^{MSS/sulf}$ is highly sensitive to temperature and metal/S of the MSS (Li et al. 1996; Ballhaus et al. 2001) and our estimated $D_{Ni}^{MSS/sulf}$ is similar to values documented in previous As-bearing experiments ($D_{Ni}^{MSS/sulf}$ 0.9-2.6 Bai et al. 2017; 0.5-2.2 Helmy et al. 2013a) and As-free sulfide systems (Li et al. 1996; Ballhaus et al. 2001) at similar temperature and metal/S ratios conditions. Cobalt is more compatible ($D_{Co}^{MSS/sulf}$ = 1.73 ± 0.07) in MSS than Ni. As expected, Cu resulted to be strongly incompatible in MSS ($D_{Cu}^{MSS/sulf}$ = 0.18 ± 0.02 at 1000 ºC). This value is also very similar to results from As-bearing sulfide systems ($D_{Cu}^{MSS/sulf}$ 0.22 ± 0.03 Bai et al. 2017; 0.21-0.26 Helmy et al. 2013a; ~ 0.2 Sinyakova and Kosyakov 2012) and fall within the range reported by Mungall et al. (2005) at 1050 ºC ($D_{Cu}^{MSS/sulf}$ = 0.22), under fS_2 typical of natural sulfide magmas.

At 1000 ºC, Os and Ru are compatible into MSS with $D^{MSS/sulf}$ values of 4.6 ± 2.1 and 6.3 ± 2.0, respectively, whereas Pt and Pd are strongly incompatible showing $D^{MSS/sulf}$ values of 0.07 ± 0.07 and 0.19 ± 0.13, respectively. Iridium is equally distributed between MSS and sulfide melt as shown by $D_{Ir}^{MSS/sulf}$ approaching unity (1.01 ± 0.73). These values are quite similar to those reported in literature for As-free sulfide systems (Li et al. 1996; Ballhaus et al. 2001).

The 840 ºC experiment was done to observe how PGE behave during the cooling of arsenide-saturated sulfide melt. The obtained textures suggest that the arsenide melt separates into a crystalline relatively Co-rich phase and Ni-rich arsenide melt (Fig. 4c). The crystalline Co-bearing phase has an average chemical formula of $(Ni_{0.78}Fe_{0.20}Co_{0.07})_{1.05}(As_{0.90}S_{0.02})_{0.92}$, representing probably a Fe-rich nickeline (NiAs). This is consistent with previous experimental studies on the Ni-As (Yund 1961) and Fe-Ni-As (Buseck 1963) systems. The Ni-As phase diagram predicts that at As concentrations similar to those of our arsenide melt at 1000 ºC, nickeline would be the first mineral to crystallize at temperatures ranging from 900 to 850 ºC. Similarly, Buseck (1963)'s phase diagram at 800 ºC predicts that Ni arsenide melts would decompose upon cooling into nickeline and maucherite. Buseck (1963) also documented an extensive but incomplete solid solution between FeAs and $Ni_{1\pm x}As$ and observed that an increasing Fe content depresses the amount of As that can enter the structure. Thus, the presence of Fe may explain the low As content of Co-bearing nickeline-type phase with 3-4 wt. % less As than stoichiometric value. The IPGE (Os, Ir, Ru) are compatible in the crystalline arsenide phase with $D^{(\text{arsenide phase/arsenide melt})}$ around 4 (Table 3). By contrast, Pt and Pd are incompatible in the Co-rich phase with D_{Pt} and D_{Pd} of 0.6 and 0.2, respectively.

Discussion

Previous experimental studies have shown that Pt and As can self-organize to nanoparticles at temperatures above 1180 ºC well before arsenide saturation is reached (Helmy et al. 2013b). If these Pt-As nano-associations, or alternatively any other association formed by PGE-ligand, had formed in our experimental systems, these nanophases would have been identified in the run products by the observations carried out by Field Emission Scanning Electron Microprobe whose resolution reaches nanometer particle sizes. However, no PGE-As nano-associations were found and thus PGE are considered to occur in solid solution within run product phases, particularly into arsenide phases.

The experiments prove that all PGE have high affinity for arsenide liquids. In particular, experiments have showed that Pt and Ir ($D^{As/sulf}{}_{Pt,Ir}$ ~ 100-2700) fractionate more strongly to arsenide melts than Os and Ru ($D^{As/sulf}{}_{Ru,Os}$ ~ 30-100), whereas Pd has low partition coefficients at 1200 and 1100 ºC ($D^{As/sulf}{}_{Pd}$ ~ 30) and relatively high at 1000 ºC ($D^{As/sulf}{}_{Pd}$ ~ 475). The obtained partition coefficients are in the range of those inferred from natural samples (Godel et al. 2012; Hanley 2007; Piña et al. 2013, 2015). Particularly, our results are quite in agreement with the partition coefficients estimated by Piña et al. (2013) using PGE abundances in co-existing arsenide and sulfide minerals from the Amasined Ni-Cu ores, North Morocco (Fig. 8). Although there is some difference in some quantitative values (for example, Ir and Pt), in both cases the partition coefficients of Os and Ru are significantly lower than that of Ir, and the partition coefficient of Pt is higher than that of Pd. In addition, it is probable that the difference in the $D_{Pt}{}^{As/sulf}$ between our exp1000 and that estimated by Piña et al. (2013) is not so large since the D value obtained by Piña et al. represents a minimum estimation and is probably higher. This figure also shows that D values of PGE increases with decreasing temperature. We suggest that this is due to the more efficient separation of arsenide and sulfide melt in the experiments with decreasing temperature. The calculated partition coefficients imply that the formation of arsenide melt can exert a major control on the PGE distribution in a given magmatic sulfide deposit. Following, we discuss the formation of arsenide melts by immiscibility liquid from sulfide magmas and consider the variable D values between arsenide and sulfide melts as responsible of PGE fractionation in natural As-rich ore deposits.

Arsenide melt immiscibility from sulfide melts

The As content of typical basaltic magmas is very low, around 0.1 ppm (Jenner et al. 2010). Despite this low As content, some magmatic ore deposits in mantle-derived rocks contain wt. % levels of As (e.g., Ronda, Spain; Beni Bousera, Morocco; Dundonald Beach South, Canada, Rosie Nickel prospect, Australia), suggesting that an effective mechanism of As enrichment and concentration must have taken place during the magmatic evolution of these systems. The partition coefficient of As between sulfide and basaltic melt is in the range of 25 to 32 (Kiseeva et al. 2017). This relatively high $D_{As}^{sulfide\ melt/basaltic\ melt}$ implies that As will partition into the sulfide melt segregating from basaltic magma. As a consequence, typical mantle sulfide melts contain up to 70 ppm As, with some Ni-rich mantle sulfides having values as high as 670 ppm (Hattori et al. 2002). Nevertheless, these values are well below the amount of As required for saturation in an arsenide phase (melt or solid) to be reached (between 0.1 and 1.5 wt. % As - Fleet et al. 1993; Helmy et al. 2013). Arsenic behaves incompatibly during sulfide melt fractionation ($D_{As}^{MSS/sulfide\ melt} = 0.40 – 0.01$, Helmy et al. 2010), which will lead to an increase in its concentration in the residual sulfide liquid. In addition, the capacity of sulfide melt to dissolve As decreases with falling temperature (~ 0.3 wt. % As and 0.5 wt. % Pt at 910 ºC, Bai et al. 2017, and 400 ppm at 770 ºC, Helmy et al. 2013a), so both phenomena may trigger the separation of an immiscible arsenide melt or the direct crystallization of arsenide phases from the sulfide melt (Helmy et al. 2013b). However, in most cases, the initial concentration of As in magmatic sulfides is too low for As saturation to be reached, even after extensive sulfide fractionation has taken place.

Consequently, it seems evident that As-enrichment at levels necessary for arsenide immiscibility to occur is only possible when the magma becomes unusually enriched in As due probably to the addition of As from an external As-rich source.

Crustal contamination with As-rich lithologies has been suggested for several magmatic arsenide occurrences (e.g., Dundonald Beach South, Canada, Hanley 2007; Rosie Nickel prospect, Australia, Godel et al. 2012; Wannaway Ni sulfide deposit, Australia, Moroni et al. 2017). At the Rosie Nickel prospect, Godel et al. (2012) suggested that significant amounts of As were added to magma by the thermomechanical erosion of komatiite flows and assimilation of organic matter-rich black shales. Similarly, at the Dundonald Beach South deposit, Hanley (2007) concluded that komatiite magmas were contaminated with organic-rich shale rocks with high As/Sb ratios leading to the segregation of an arsenide melt. At the Wannaway komatiite-hosted Ni sulfide deposit, Moroni et al. (2017) indicated that sulfidic shales containing accessory As and Te sulfosalts were the source of As via contamination of sulfide melts. Gervilla et al. (1998) also suggested that arsenide melt segregation in Kylmaköski (Finland) resulted from contamination of parental silicate magma with As-rich Svecofenian metasediments (Lahtinen and Lestinen 1996). In conclusion, crustal contamination of mantle magma with As-rich materials can increase the As content of magma to the point that they become saturated in an arsenide phase, i.e. thousands of ppm.

PGE fractionation in natural As-rich orebodies

The high $D_{PGE}^{arsenide\ melt/sulfide\ melt}$ estimated in this study explain the enrichment of PGE in those As-rich parts relative to the As-poor parts from arsenide-rich natural sulfide ores. However, the values of D cannot explain by themselves the fractionation of Pt and

Pd from Or, Ir, Ru and Rh observed in some arsenide-rich sulfide deposits. Indeed, partition coefficient values for Os-Ir-Ru are not very different to those for Pd-Pt (Table 3), and arsenide minerals tend to be particularly enriched in Pt and Pd relative to Os, Ir, Ru and Rh. Furthermore, Pd is typically the most abundant PGE in the As-rich sulfide deposits, with Pt/Pd ratios usually below unity (*e.g.*, Hanley, 2007), and $D_{Pd}^{As\text{-}melt/sulf\text{-}melt}$ is significantly lower than $D_{Pt}^{As\text{-}melt/sulf\text{-}melt}$. Alternatively, the fractionation of PGE can be due to factors such as the timing of arsenide melt segregation (*i.e.*, before or after MSS fractionation), and saturation in PGE arsenide minerals. Additionally, our experiment at 840 ºC shows that Os, Ir and Ru are fractionated from Pt and Pd during the arsenide melt crystallization with the former metals being preferentially concentrated in the Co-bearing nickeline, whereas Pt and Pd are concentrated in the residual arsenide melt.

a) *Timing of arsenide melt segregation*. The enrichment of Pd and Pt relative to IPGE can be the result of different timing in the arsenide melt segregation, namely before or after MSS crystallization. If arsenide-sulfide immiscibility occurs after MSS crystallization, such as is suggested for Kylmäkoski, Vammala and Talnotry (Gervilla et al. 1998; Power et al. 2004), arsenide melt will scavenge only those PGE incompatible in MSS, Pt and Pd, because Os, Ir, Ru and Rh were incorporated into MSS owing to their higher compatibility in this phase. As a result, arsenide and sulfarsenide minerals are all depleted in IPGE relative to Pd and Pt. By contrast, if arsenide melt separates before MSS crystallization, Os, Ir, Ru and Rh are also concentrated into the arsenide melt along with Pt and Pd and the arsenide-bearing orebodies are not fractionated in terms of Pd-Pt versus Os-Ir-Ru-Rh. This has been suggested for Beni Bousera (Morocco), Ronda (Spain) (Piña et al. 2013, 2015), and the Wannaway komatiite-hosted

Ni sulfide deposit, Kambalda (Moroni et al. 2017). In this last case, gersdorffite and irarsite crystallized from an arsenide melt segregated from sulfide melt before MSS crystallization took place at a temperature higher than 1200 ºC and are enriched in all PGE up to wt. % levels. In the case of Beni Bousera and Ronda, nickeline and maucherite formed by crystallization of arsenide melt segregated before MSS formation, incorporated all PGE, whereas pyrrhotite and pentlandite, which formed after MSS decomposition, have very low Os, Ir and Ru contents.

b) Early-crystallization of discrete arsenide minerals. Helmy and Bragagni (2017) observed that PGE show different chemical affinities for As in the As-PGE-sulfide system above 1200 ºC: Pt and Pd tend to form diarsenides, Ir and Rh form sulfarsenides (irarsite IrAsS, and hollingworthite RhAsS), while Ru and Os tend to form discrete sulfides and alloys, respectively. The depletion of As-rich portions of sulfide deposits in IPGE could be an original chemical feature of the sulfide liquid before arsenide-melt separation. Probably, IPGE fractionate early in the form of IPGE alloys or sulfides incorporated in oxides and silicates as suggested by Helmy and Bragagni (2017). Similarly, Pt tends to form stable stoichiometric arsenides at magmatic temperatures (sperrylite, Helmy et al, 2013b), which is also not uncommon in chromite-rich ores. If Pt is extracted from sulfide melt in the form of early-formed sperrylite later incorporated in silicate and/or oxides, any arsenide melt segregated later will be relatively enriched in Pd relative to Pt. In addition, Pd is also the most incompatible PGE during normal sulfide melt fractionation and is highly enriched in the Cu-rich residual sulfide melt. It could well be that the low Pt/Pd ratios in some deposits are the result of both Pd enrichment in the residual sulfide melt and the strong early fractionation of Pt into discrete minerals (e.g., sperrylite) once As becomes and important component.

c) Crystallization and phase separation during arsenide melt fractionation. The experiment that was slowly cooled to 840 ºC shows that Co-bearing nickeline is the early Ni-arsenide phase to crystallize from an arsenide melts such as has been observed in natural occurrences (e.g., Ronda). Osmium, Ir and Ru dissolved in the arsenide melt behave compatibly during the separation of this phase, whereas Pt and Pd remain in the residual arsenide melt. This implies that during the cooling of the arsenide melt and the crystallization of Co-bearing phases, further fractionation of IPGE over Pt and Pd will take place. In addition, the difference in D_{Pt} and $D_{Pd}^{(Co\text{-}bearing\ nickeline/arsenide\ melt)}$ (i.e., 0.6 and 0.2, respectively) may be enough to shift Pd/Pt ratio as arsenide-phases fractionate from the arsenide melt.

Implications for PGE metallogenesis

Platinum group elements are all strongly compatible into arsenide melts with $D_{PGE}^{arsenide\ melt/sulfide\ melt}$ ranging from 20 to 2700. Thus, the formation of arsenide melts by immiscibility from As-rich sulfide melts, regardless of the processes causing the increase in As content, can lead to the PGE concentration in As-PGE-rich orebodies or horizons in magmatic sulfide deposits. These orebodies formed by PGE-rich arsenide and sulfarsenide minerals will coexist with S-rich and PGE-poor orebodies formed from PGE-depleted sulfide melts. Factors such as the timing of arsenide melt segregation and the saturation in PGE arsenide minerals previously to the arsenide melt immiscibility will play an important role in fractionating of PGE into orebodies. If arsenide melt segregates before MSS crystallization, arsenide melt will concentrate all PGE and the resulting As-rich orebodies will be enriched in these elements leaving S-rich orebodies impoverished in these precious metals. By contrast, if arsenide melt segregates after MSS crystallization, the As-rich orebodies will be only enriched in those PGE incompatible into MSS (Pd, and Pt) because IPGE and Rh have been previously incorporated into the MSS due to their compatibility in this phase. Finally, our results indicate that the fractionation of Co-bearing arsenide phases from arsenide melts during cooling will have the same effect than MSS fractionation from sulfide melt on the fractionation of IPGE from PPGE.

Acknowledgements This research was supported by Spanish project RTI2018-099157-A-100. Raúl Fonseca is grateful to the Deutsche Forchungsgemeinschaft for funding of a Heisenberg Professorship (via grant FO 698). We also wish to thank Alfredo Larios (ICTS National Centre for Electron Microscopy, Complutense University of Madrid) for his assistance with the electron microprobe analyses and photomicrographs. We very much appreciate the comments from the reviewers James Brenan and Yuan Li, and Associate Editor Kate Kiseeva, who significantly improved the manuscript.

References

Bai, L., Barnes, S-J., and Baker, D.R. (2017) Sperrylite saturation in magmatic sulfide melts: Implications for formation of PGE-bearing arsenides and sulfarsenides. American Mineralogist, 102, 966-974.

Ballhaus, C., Tredoux, M., and Späth, A. (2001) Phase relations in the Fe-Ni-Cu-PGE-S system at magmatic temperature and application to massive sulphide ores of the Sudbury Igneous Complex. Journal of Petrology, 42, 1911-1926.

Bragagni, A., Van Acken, D., Fonseca, R.O.C., Speelmanns, I.M., Wainwright, A.N., Heuser, A., Nowell, G.M., and Luguet, A. (2018) Re-Os and HSE in individual base metal sulfide grains: Evaluating micro-analytical procedures using a sulfide reference material. Chemical Geology, 493, 426-440.

Buseck, P.R. (1963) The Fe-Ni-As system at 800ºC. Carnegie Inst. Washington Year Book 62: 200-210

Canali, A.C., Brenan, J.M., Sullivan, N.A. (2017) Solubility of platinum-arsenide melt and sperrylite in synthetic basalt at 0.1 Mpa and 1200 ºC with implications for arsenic speciation and platinum sequestration in mafic igenous systems. Geochimica et Cosmochimica Acta, 216, 153-168.

Evans, D.M., Bymelwa, L., Gilligan, J. (1999) Variability of magmatic sulphide compositions at the Kabanga nickel prospect, Tanzania. Journal of African Earth Sciences, 29, 329-351.

Fleet, M.E., Chryssoulis, S.L., Stone, E.S., and Weisener, C.G. (1993) Partitioning of platinum-group elements and Au in the Fe-Ni-Cu-S system. Experiments on the fractional crystallization of sulfide melt. Contributions to Mineralogy and Petrology, 115, 36-44.

Fonseca, R.O.C., Campbell, I.H., O'Neill, H.St.C., and Allen, C.M. (2009) Solubility of Pt in sulphide mattes: Implications for the genesis of PGE-rich horizons in layered intrusions. Geochimica et Cosmochimica Acta, 73, 5764−5777.

Fonseca, R.O.C., Mallmann, G., O'Neill, H.St.C., Campbell, I.H., and Laurenz, V. (2011) Solubility of Os and Ir in sulfide melt: Implications for Re/Os fractionation during mantle melting. Earth and Planetary Science Letters, 311, 339−350.

Fonseca, R.O.C., Laurenz, V., Mallmann, G., Luguet, A., Hoehne, N., and Jochum, K.P. (2012) New constraints on the genesis and long-term stability of Os-rich alloys in the Earth's mantle. Geochimica et Cosmochimica Acta, 87, 227−242.

Gervilla, F., and Leblanc, M. (1990) Magmatic ores in high-temperature alpine-type lherzolite massifs (Ronda, Spain, and Beni Bousera, Morocco). Economic Geology, 85, 112-132.

Gervilla, F., Leblanc, M., Torres-Ruiz, J., and Fenoll Hach-Alí, P. (1996) Immiscibility between arsenide and sulfide melts: a mechanism for the concentration of noble metals. Canadian Mineralogist, 34, 485-502.

Gervilla, F., Papunen, H., Kojonen, K., and Johanson, B. (1998) Platinum-, palladium- and gold-rich arsenide ores from the Kylmäkoski Ni-Cu deposit (Vammala Nickel Belt, SW Finland). Mineralogy and Petrology, 64, 163-185.

Gervilla, F., González-Jiménez, J.M., Hidas, K., Marchesi, C., and Piña, R. (2019) Geology and Metallogeny of the Upper Mantle Rocks from the Serranía de Ronda. Mineralogical Spanish Society, Ronda, p 122

Godel, B., González-Álvarez, I., Barnes, S.J., Barnes, S-J., Parker, P., and Day, J. (2012) Sulfides and sulfarsenides from the Rosie Nickel Prospect, Duketon Greenstone Belt, Western Australia. Economic Geology, 107, 275-294.

Hanley, J.J. (2007) The role of arsenic-rich melts and mineral phases in the development of high-grade Pt-Pd mineralization within komatiite-associated magmatic Ni-Cu sulfide horizons at Dundonald Beach South, Abitibi subprovince, Ontario, Canada. Economic Geology, 102, 305-317.

Hattori, K.M., Arai, S., and Clarke, D.B. (2002) Selenium, tellurium, arsenic and antimony contents of primary mantle sulfides. Canadian Mineralogist, 40, 637-650.

Helmy, H.M., Ballhaus, C., Wohlgemuth-Ueewasser, C., Fonseca, R., and Laurenz, V. (2010) Partitioning of Se, As, Sb, Te and Bi between monosulfide solid solution and sulfide melt—application to magmatic sulfide deposits. Geochimica et Cosmochimica Acta, 74, 6174−6179.

Helmy, H.M., Ballhaus, C., Fonseca, R.O.C., and Nagel, T.J. (2013a) Fractionation of platinum, palladium, nickel, and copper in sulfide-arsenide systems at magmatic temperature. Contributions to Mineralogy and Petrology, 166, 1725-1737.

Helmy, H.M., Ballhaus, C., Fonseca, R.O.C., Wirth, R., Nagel, T., and Tredoux, M. (2013b) Noble metal nanoclusters and nanoparticles precede mineral formation in magmatic sulfide melts. Nature Communications, 4, 2405.

Helmy, H.M., and Bragagni, A. (2017) Platinum-group elements fractionation by selective complexing: the Os, Ir, Ru, Rh arsenide-sulfide systems above 1020ºC. Geochimica et Cosmochimica Acta, 216, 169-183.

Helmy, H.M., and Fonseca, R.O.C. (2017) The behavior of Pt, Pd, Cu and Ni in the Se-sulfide system between 1050 and 700° C and the role of Se in platinum-group elements fractionation in sulfide melts. Geochimica et Cosmochimica Acta, 216, 141-152.

Jenner, F.E., O'Neill, H.S.C., Arculus, R.J., and Mavrogenes, J.A. (2010) The magnetite Crisis in the Evolution of Arc-Related Magmas and the Initial Concentration of Au, Ag and Cu. Journal of Petrology, 51, 2445–2464.

Jochum, K.P., Weis, U., Stoll, B., Kuzmin, D., Yang, Q., Raczek, I., Jacob, D.E., Stracke, A., Birbaum, K., Frick, D.A., Günther, D., and Enzweiler, J. (2011) Determination of reference values for NIST SRM 610-617 glasses following ISO guidelines. Geostand Geoanal Res, 35, 397–429.

Kiseeva, E.S., Fonseca, R.O.C., and Smythe, D.J. (2017) Chalcophile elements and sulfides in the Upper Mantle. Elements, 13, 111-116.

Lahtinen, R., and Lestinen, P. (1996) Background variations of ore-related elements and regional scale mineralization indications in Paleoproterozoic bedrock in the Tampere area, southern Finland. Geol Surv Finland Bull 390:1-34

Leblanc, M., Gervilla, F., and Jedwab, J. (1990) Noble metals segregation and fractionation in magmatic ores from Ronda and Beni Bousera lherzolite massifs (Spain, Morocco). Mineralogy and Petrology, 42, 233-248.

Li, C., Barnes, S-J., Makovicky, E., Rose-Hansen, J., and Makovicky, M. (1996) Partitioning of nickel, copper, iridium, rhenium, platinum, and palladium between monosulfide solid solution and sulfide liquid: Effects of composition and temperature. Geochimica et Cosmochimica Acta, 60, 1231−1238.

Liu, Y., and Brenan, J. (2015) Partitioning of platinum-group elements (PGE) and chalcogens (Se, Te, As, Sb, Bi) between monosulfide-solid solution (MSS), intermediate solid solution (ISS) and sulfide liquid at controlled fO2–fS2 conditions. Geochimica et Cosmochimica Acta, 159, 139–161.

Makovicky, E., Karup-Moller, S., Makovicky, M., and Rose-Hansen, J. (1990) Experimental studies on the phase systems Fe-Ni-Pd-S and Fe-Pt-Pd-As-S applied to PGE deposits. Mineralogy and Petrology, 42, 307-319.

Makovicky, M., Makovicky, E., and Rose-Hansen, J. (1992) The phase system Fe-Pt-As-S at 850ºC and 470ºC. Neues Jahrb Mineral, 10, 441-453.

Mengason, M.J., Piccoli, P.M., and Candela, P. (2010) An evaluation of the effect of copper on the estimation of sulfur fugacity (fS2) from pyrrhotite composition. Economic Geology, 105, 1163–1169.

Moroni, M., Caruso, S., Barnes, S.J., and Fiorentini, M. (2017) Primary stratigraphic controls on ore mineral assemblages in the Wannaway komatiite-hosted nickel-sulfide deposit, Kambalda camp, Western Australia. Ore Geology Reviews, 90, 634-666.

Mungall, J.E., Andrews, R., Cabri, L.J., Sylvester, P.J., and Tubrett, M. (2005) Partitioning of Cu, Ni, An, and platinum-group elements between monosulfide solid solution and sulfide melt under controlled oxygen and sulfur fugacities. Geochimica et Cosmochimica Acta, 69, 4349–4360.

Oen, I.S., Kieft, C., and Westerhof, A.B. (1979) Variation in composition of chromites from chromite-arsenide deposits in peridotites of Málaga, Spain. Economic Geology, 74, 1630-1636.

Piña, R., Gervilla, F., Barnes, S-J., Ortega, L., and Lunar, R. (2013) Partition coefficients of platinum-group and chalcophile elements between arsenide and sulfide phases as determined in the Amasined sulfide-graphite mineralization (Beni Bousera, North Morocco). Economic Geology, 108, 935-951.

Piña, R., Gervilla, F., Barnes, S-J., Ortega, L., and Lunar, R. (2015) Liquid immiscibility between arsenide and sulfide melts: evidence from a LA-ICP-MS study in magmatic deposits at Serranía de Ronda (Spain). Mineralium Deposita, 50, 265-279.

Power, M.R., Pirrie, D., Jedwab, J., and Stanley, C.J. (2004) Platinum-group element mineralization in an As-rich magmatic sulfide system, Talnotry, southwest Scotland. Mineralogical Magazine, 68, 395-411.

Sinyakova, E.F., and Kosyakov, V.I. (2012) The behavior of noble-metal admixtures during fractional crystallization of As- and Co-containing Cu-Fe-Ni sulfide melts. Russ Geol Geophys, 53, 1055–1076.

Tomkins, A.G. (2010) Wetting facilitates late-stage segregation of precious metal–enriched sulfosalt melt in magmatic sulfide systems. Geology, 38, 951-954.

Toulmin, P., and Barton, Jr. P.N. (1964) A thermodynamic study of pyrite and pyrrohtite. Geochimica et Cosmochimica Acta, 28, 641– 671.

Wood, M. (2003) Arsenic in igneous systems: An experimental investigation. Unpublished BA Sc thesis, Toronto, Canada, University of Toronto, 32 p

Yund, R.A. (1961) Phase relations in the system Ni-As. Economic Geology, 56, 1273-1296

Figure captions

Figure 1. Reflected-light optical microscope photographs showing: a) chromite-bearing sulfide layer interbedded with chromite-bearing nickelite-(löllingite) layer; b) Maucherite grains coexisting with pyrrhotite included between chromite crystals; c) Maucherite grains with curved boundaries including small chromite crystals in pyrrhotite; and d) Subrounded maucherite grains hosted by pyrrhotite and surrounded by thin rims of cobaltite-gersdorffite. Photographs a and b are from the Cr-Ni ores at La Gallega Mine in the Serranía de Ronda, Spain, and photographs c and d are from the Amasined Cr-Ni mineralization in the Beni Bousera ultramafic massif, Morocco.

Figure 2. Phase relations of the experiments in back-scattered electron (BSE) mode. a-b) Arsenide melt (*bright*) showing dendritic textures within a matrix of sulfide melt (*grey*); experiment products at 1200 ºC. c-d) Fine-grained arsenide melt droplets predominate over hundred micrometer-sized rounded droplets within sulfide melt in the experimental run products at 1100 ºC. e-f) Rounded arsenide droplets coexisting with MSS and sulfide liquid. Observe that sulfide liquid is located interstitially into

MSS and the presence of minute arsenide melt droplets within sulfide liquid not present within MSS.

Figure 3. Microphotograph taken by reflective-light optical microscope showing the boundary between arsenide and sulfide melts in the run product at 1200 ºC. Observe the presence of “blebs” of arsenide melt migrating to the larger bleb of arsenide melt.

Figure 4. Phase relations of the experiments in back-scattered electron (BSE) mode. a-b) Run products at 840 ºC with two different arsenide phases (light grey: Co-rich arsenide phase; dark grey: Ni-rich arsenide phase) coexisting with MSS (black) and ISS (grey).

Figure 5. Compositional maps showing the distribution of Fe, S, Co, As, Ni and Cu obtained by electron microprobe for coexisting phases at 1100 ºC (a), 1000 ºC (b), and 840 ºC (c).

Figure 6. Distribution of Ni (a), Co (b), S (c), Fe (d), As (e) and Cu (f) between coexisting phases at different temperature run conditions. The dashed line represents the initial concentration of the starting material. Error bars are 2σ of the mean.

Figure 7. Distribution of Os (a), Ir (b), Ru (c), Pt (d) and Pd (e) between coexisting phases at the different temperature run conditions. The dashed line represents the initial concentration of the starting material. Error bars are σ of the mean.

Figure 8. Partition coefficients of PGE between arsenide and sulfide melts calculated in this study for 1200, 1100, and 1000 ºC in comparison with partition coefficients estimated by Piña et al. (2013) in natural samples from the Amasined Ni-Cu ores (Beni Bousera, North Morocco).

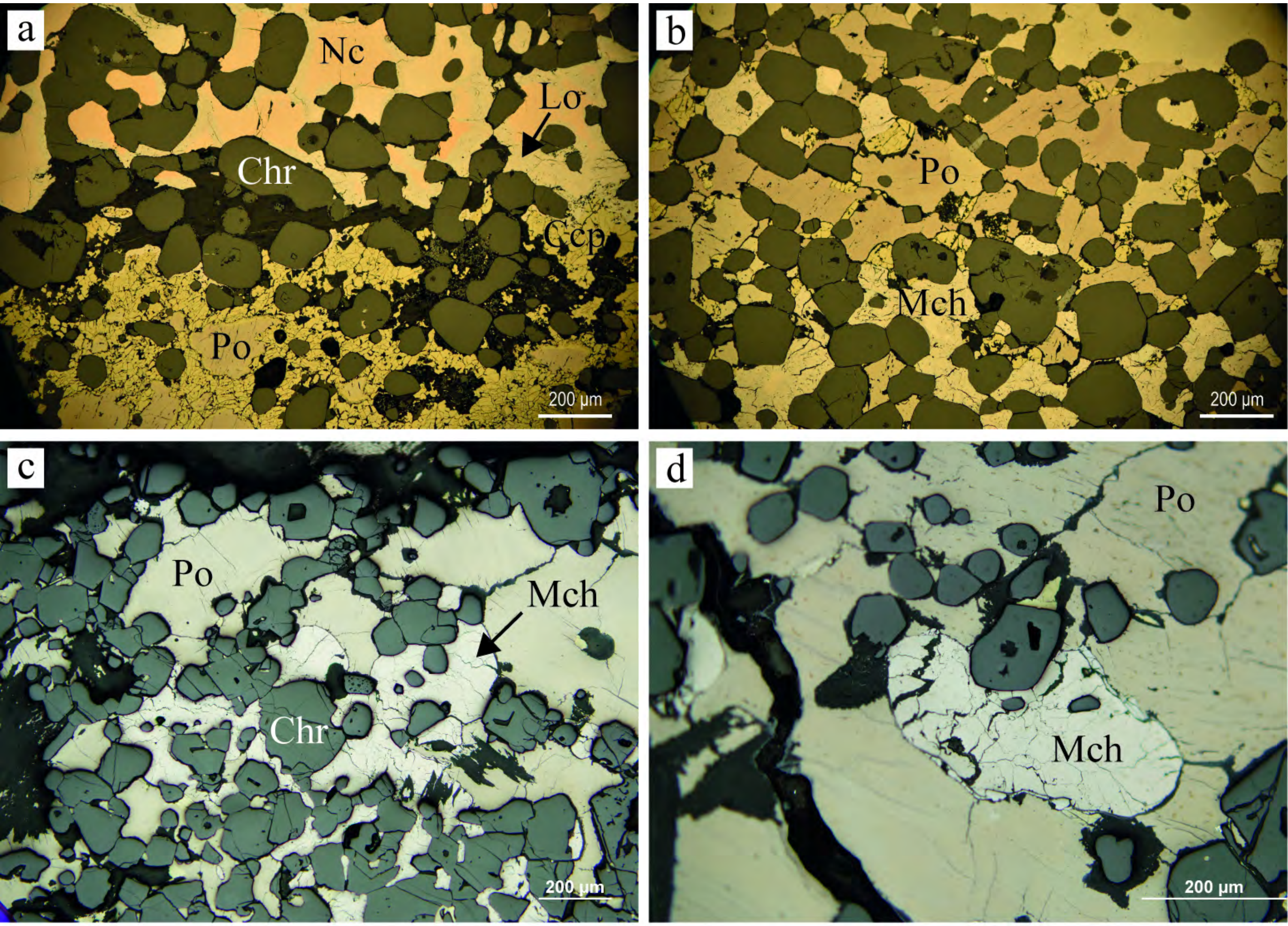
a
Nc
Lo
Chr
Ccp
Po
200 µm
b
Po
Mch
200 µm
c
Po
Mch
Chr
200 µm
d
Po
Mch
200 µm

FIGURE 1

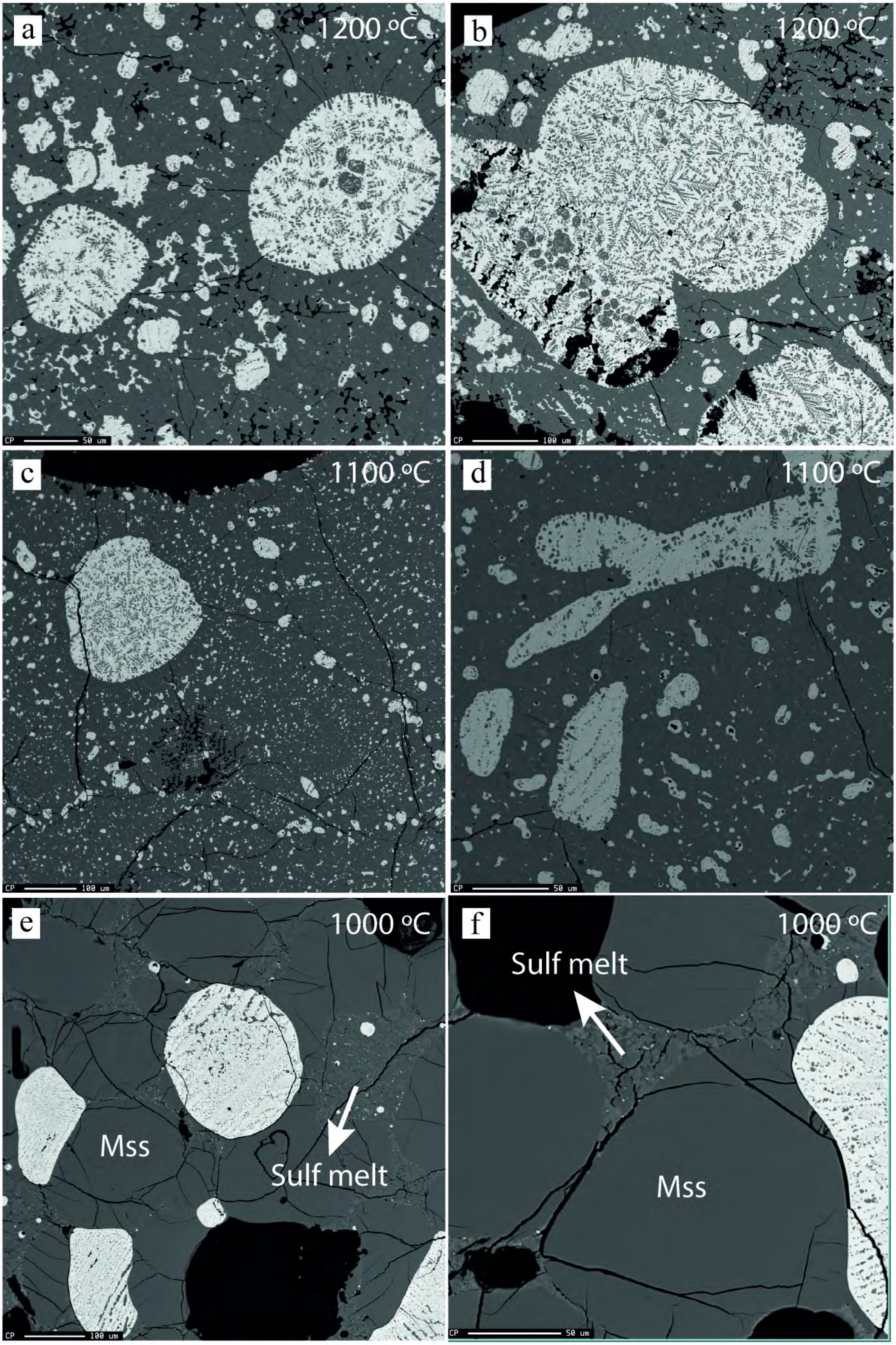
a
1200 °C
CP 50 um
b
1200 °C
CP 100 um
c
1100 °C
CP 100 um
d
1100 °C
CP 50 um
e
1000 °C
Mss
Sulf melt
CP 100 um
f
1000 °C
Sulf melt
Mss
CP 50 um

FIGURE 2

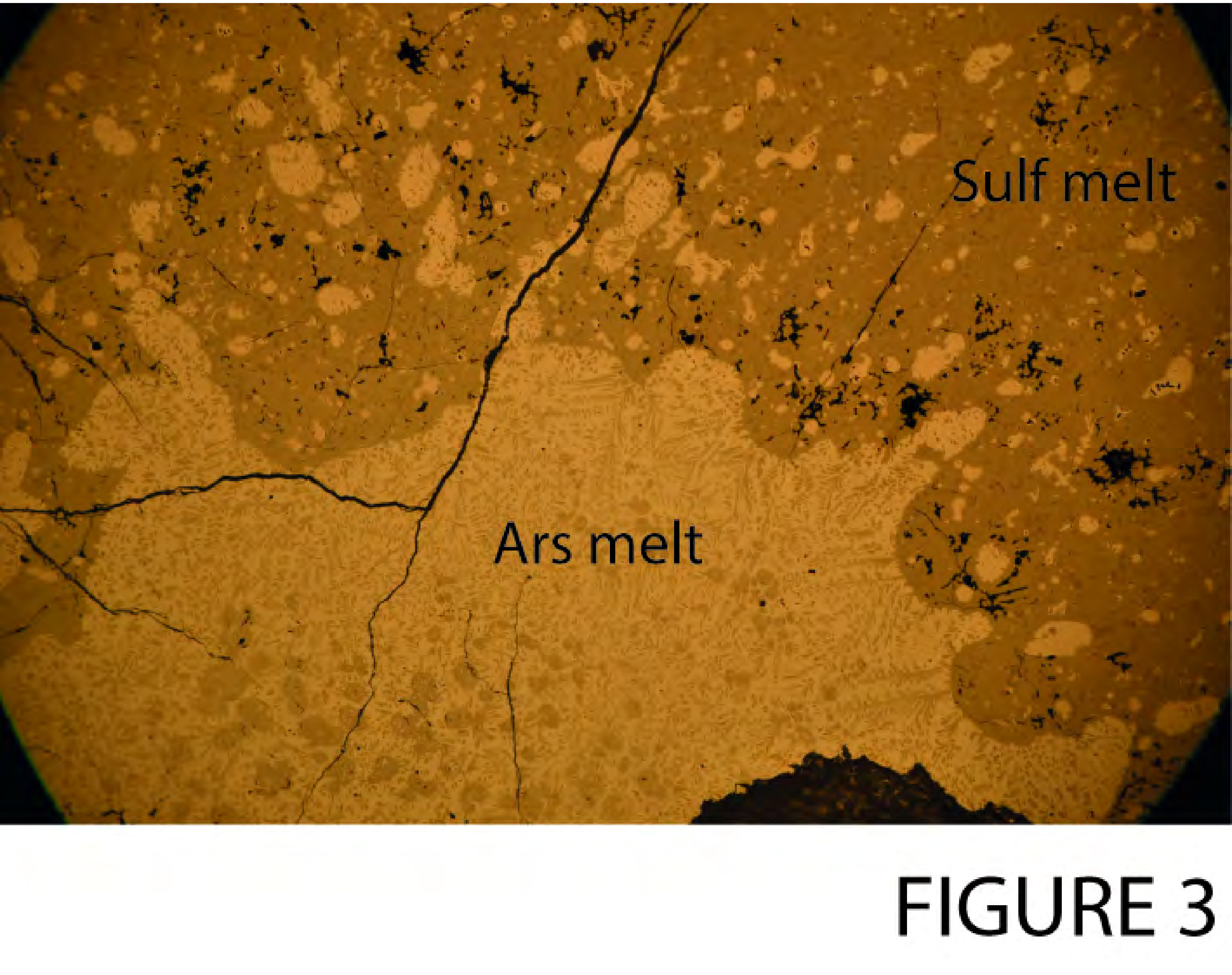

FIGURE 3

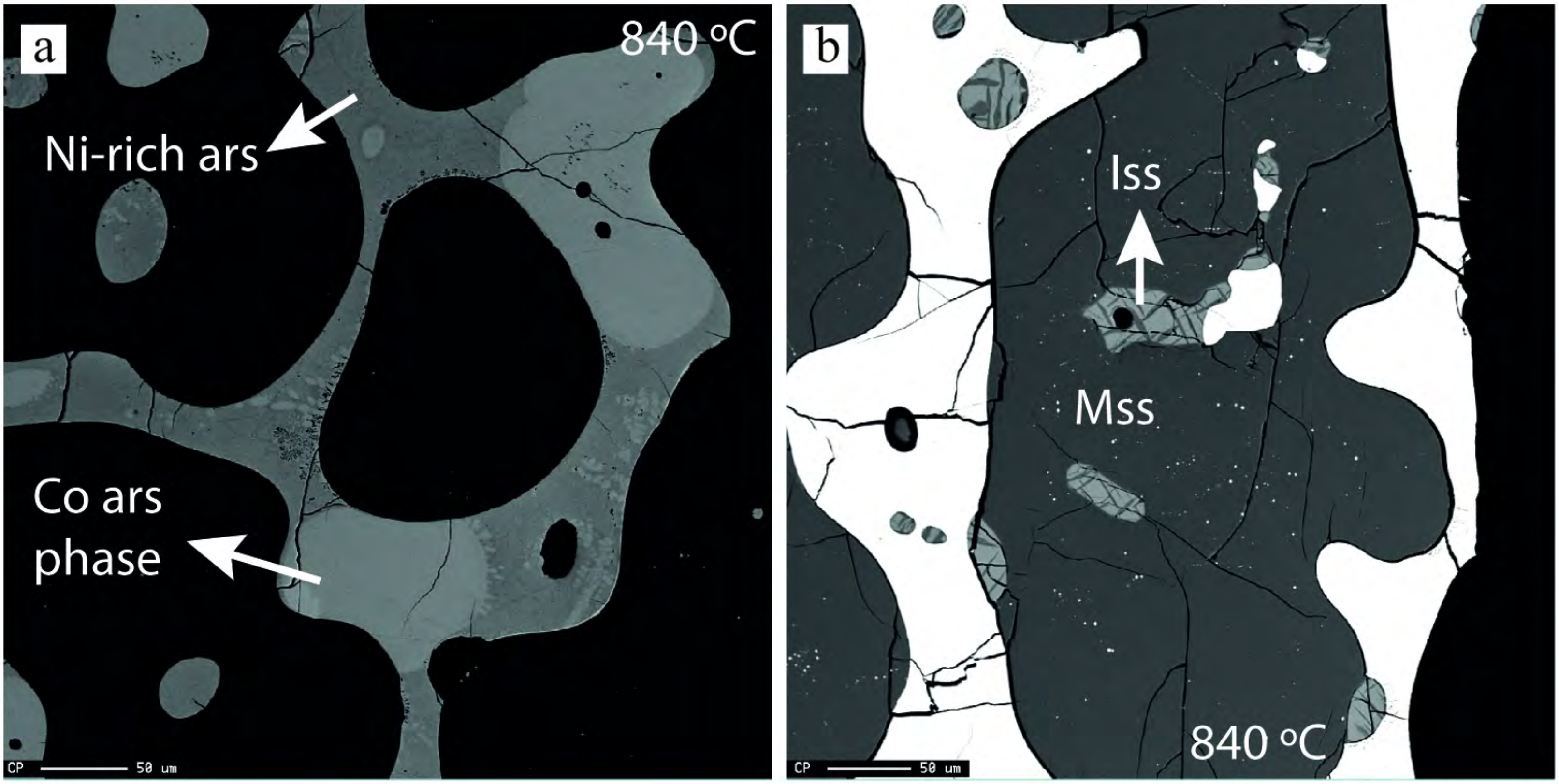

FIGURE 4

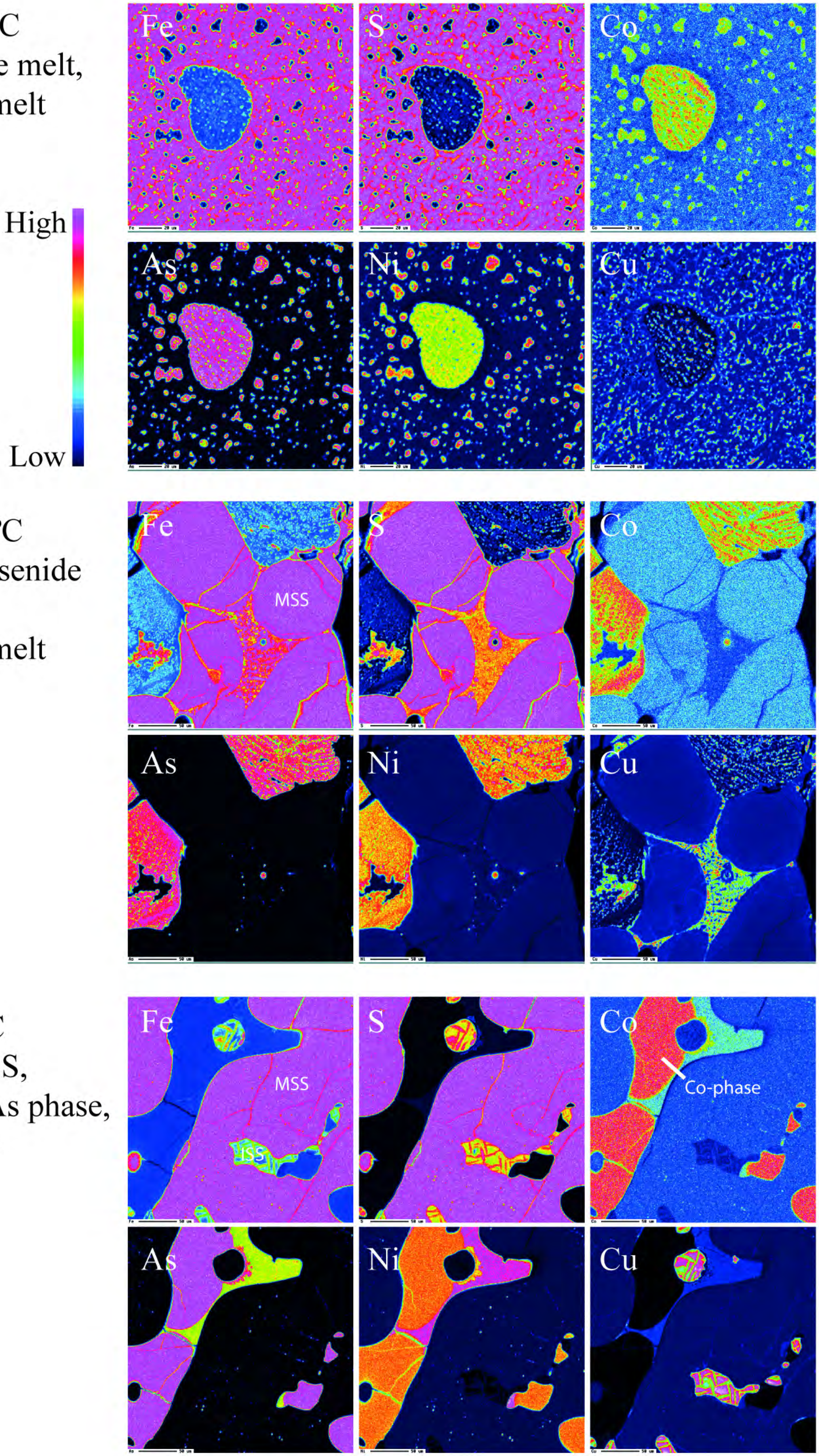

a) 1100ºC
Arsenide melt,
sulfide melt

b) 1000ºC
MSS, arsenide
melt,
sulfide melt

c) 840ºC
MSS, ISS,
Ni-Co-As phase,
arsenide
melt

FIGURE 5

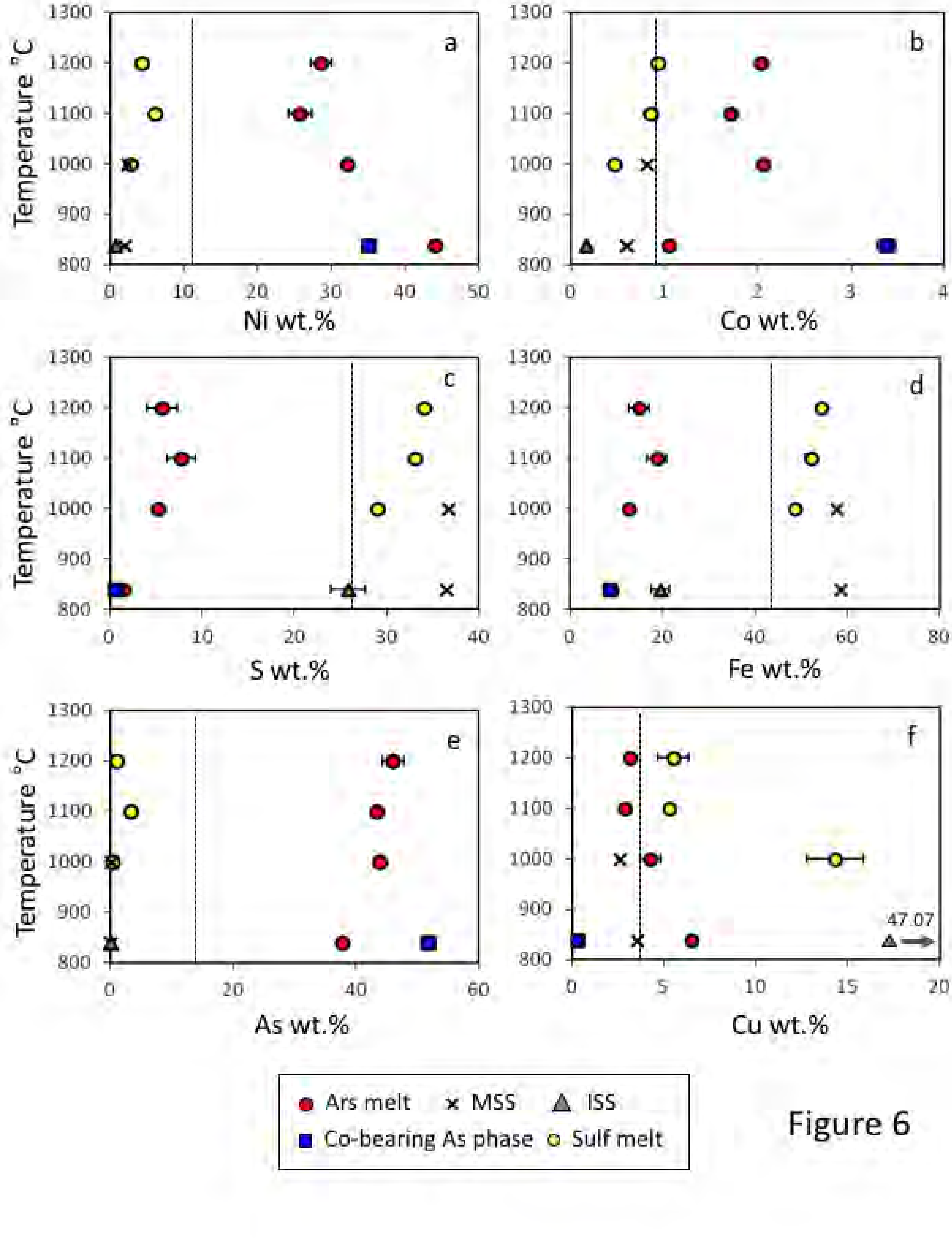

Temperature °C
1300
1200
1100
1000
900
800
a
Ni wt.%
0
10
20
30
40
50
b
Co wt.%
0
1
2
3
4
c
S wt.%
0
10
20
30
40
d
Fe wt.%
0
20
40
60
80
e
As wt.%
0
20
40
60
f
Cu wt.%
0
5
10
15
20
47.07
Ars melt
MSS
ISS
Co-bearing As phase
Sulf melt

Figure 6

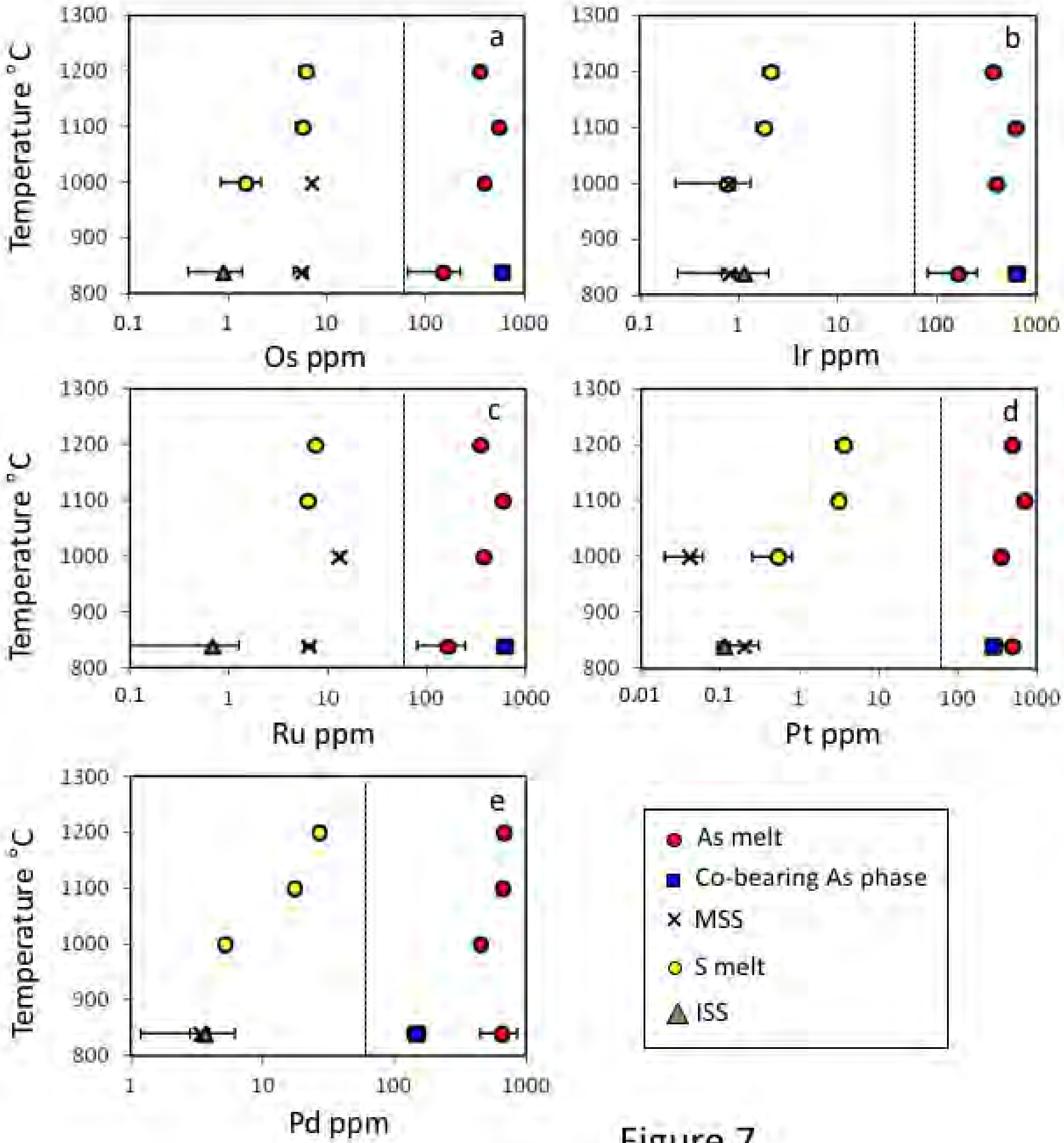
a
b
c
d
e
Temperature °C
1300
1200
1100
1000
900
800
0.01
0.1
1
10
100
1000
Os ppm
Ir ppm
Ru ppm
Pt ppm
Pd ppm
● As melt
■ Co-bearing As phase
× MSS
○ S melt
▲ ISS

Figure 7

Figure 8

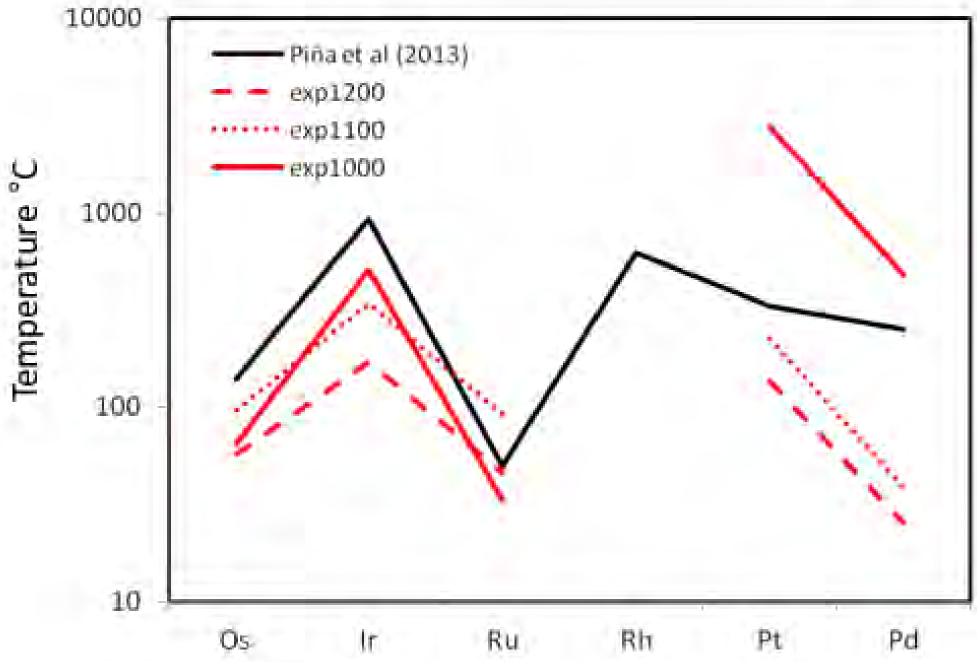
10000
1000
100
10
Temperature °C
Piña et al (2013)
exp1200
exp1100
exp1000
Os
Ir
Ru
Rh
Pt
Pd

TABLE 1. Major element compositions of run products obtained by electron microprobe

Run product	T in °C	n	Fe	Ni	Cu	Co	S	As	Total	fS_2
Ars melt	1200	8	14.87 ± 1.05	28.66 ± 0.71	3.10 ± 0.28	2.04 ± 0.02	5.65 ± 0.82	46.02 ± 0.86	100.34	
Sulf melt	1200	12	54.42 ± 0.60	4.31 ± 0.40	5.47 ± 0.42	0.93	34.09 ± 0.37	1.14 ± 0.38	100.37	
Ars melt	1100	9	18.79 ± 1.06	25.71 ± 0.80	2.87 ± 0.16	1.71 ± 0.03	7.72 ± 0.77	43.39 ± 0.94	100.19	
Sulf melt	1100	8	52.13 ± 0.60	6.10 ± 0.55	5.29 ± 0.17	0.85 ± 0.04	33.11 ± 0.39	3.37 ± 0.63	100.85	
Ars melt	1000	11	12.63 ± 0.29	32.18 ± 0.46	4.23 ± 0.28	2.06 ± 0.06	5.23 ± 0.15	43.80 ± 0.26	100.13	
MSS	1000	11	57.55 ± 0.13	2.49 ± 0.03	2.59 ± 0.10	0.81 ± 0.01	36.72 ± 0.06	0.22 ± 0.02	100.38	-3.5
Sulf melt	1000	12	48.71 ± 0.61	2.81 ± 0.11	14.30 ± 0.78	0.47 ± 0.01	29.09 ± 0.41	0.36 ± 0.04	95.77	
Ni-Co ars ph	840	10	8.44 ± 0.05	35.06 ± 0.09	0.27 ± 0.05	3.38 ± 0.05	0.60 ± 0.01	51.84 ± 0.10	99.59	
Ars melt	840	10	8.88 ± 0.11	44.05 ± 0.19	6.49 ± 0.10	1.05 ± 0.02	1.50 ± 0.05	37.83 ± 0.14	99.80	
MSS	840	10	58.40 ± 0.17	2.00 ± 0.02	3.53 ± 0.11	0.59 ± 0.02	36.49 ± 0.06	0.10 ± 0.02	101.11	-6.3
ISS	840	3	19.51 ± 1.01	0.71 ± 0.04	47.07 ± 1.50	0.16 ± 0.01	25.81 ± 0.94	0.16 ± 0.03	93.42	

Average compositions; n number of analyses; ± ranges are standard mean error. Sulfur fugacity at 1000 and 840 °C was estimated using MSS compositions according to Toulmin and Barton (1964) and Mengason et al. (2010)

TABLE 2. Platinum-group element abundances (ppm) for each run products obtained by LA-ICP-MS

Run product	T in °C	n	Os	Ir	Ru	Pt	Pd
Ars melt	1200	10	349.6 ± 20.5	364.7 ± 23.4	351.6 ± 18.8	483.4 ± 33.3	673.0 ± 50.6
Sulf melt	1200	10	6.10 ± 0.88	2.13 ± 0.37	7.64 ± 0.92	3.58 ± 0.67	26.78 ± 5.75
Ars melt	1100	10	543.7 ± 19.2	618.3 ± 23.0	582.3 ± 20.9	694.6 ± 30.8	661.5 ± 33.1
Sulf melt	1100	9	5.63 ± 0.7	1.80 ± 0.31	6.32 ± 0.74	3.11 ± 0.50	17.38 ± 2.30
Ars melt	1000	10	388.2 ± 10.9	399.4 ± 12.0	373.9 ± 10.1	353.5 ± 16.2	441.1 ± 27.4
MSS	1000	5	6.97 ± 0.14	0.79 ± 0.02	13.20 ± 0.60	0.04 ± 0.02	bdl
Sulf melt	1000	5	1.51 ± 0.65	0.77 ± 0.54	2.10 ± 0.54	0.53 ± 0.28	5.14 ± 1.13
Ni-Co ars ph	840	5	595.0 ± 89.9	634.6 ± 98.8	619.0 ± 95.2	278.8 ± 41.5	147.2 ± 22.2
Ars melt	840	5	146.6 ± 80.2	165.6 ± 85.7	162.5 ± 81.4	478.2 ± 119.7	646.6 ± 203.5
MSS	840	5	5.51 ± 0.9	0.80 ± 0.14	6.46 ± 0.75	0.2 ± 0.1	3.38 ± 0.55
ISS	840	2	0.90 ± 0.50	1.12 ± 0.88	0.69 ± 0.59	0.11 ± 0.02	3.65 ± 2.45

Average compositions; n number of analyses; ± ranges are standard mean error; bld below detection limit

Table 3. Partition coefficients of PGE, Ni, Cu, As and Co between coexisiting phases

T in °C	Os	Ir	Ru	Pt	Pd	Ni	Cu	Co	As
D arsenide melt / sulfide melt									
1200	57.3 ± 11.6	170.9 ± 40.6	46.0 ± 8.0	135.1 ± 34.7	25.1 ± 7.3	6.65 ± 0.78	0.57 ± 0.09	2.18 ± 0.02	
1100	96.6 ± 15.5	342.6 ± 72.5	92.1 ± 14.1	223.2 ± 45.7	38.1 ± 6.9	4.21 ± 0.51	0.54 ± 0.05	2.02 ± 0.14	
1000	64.9 ± 4.3	507.9 ± 88.8	33.4 ± 2.7	2751.6 ± 1559.9	475.3 ± 134.0	12.63 ± 0.42	0.90 ± 0.10	2.75 ± 0.12	
D MSS / sulf melt									
1000	4.60 ± 2.06	1.01 ± 0.73	6.29 ± 1.96	0.07 ± 0.07	0.19 ± 0.13	0.89 ± 0.05	0.18 ± 0.02	1.73 ± 0.07	0.62 ± 0.12
D Co-rich ph / arsenide melt									
840	4.06 ± 2.83	3.83 ± 2.58	3.81 ± 2.49	0.58 ± 0.23	0.23 ± 0.11	0.80 ± 0.01	0.04 ± 0.01	3.22 ± 0.13	1.37 ± 0.01